Contents lists available at UGC-CARE

International Journal of Pharmaceutical Sciences and Drug Research

[ISSN: 0975-248X; CODEN (USA): IJPSPP]

Available online at www.ijpsdronline.com

Research Article

Design of Molecular Inhibitors against the NuoC Protein of *Mycobacterium tuberculosis*

Hareesh R. Badepally[1], Lavanya Rumandla[1], Mounika Badineni[1], Ramesh Malikanti[1], Rajender Vadija[2], Kiran K. Mustyala[3], Vasavi Malkhed[4*]

[1]*Department of Chemistry, Osmania University, Hyderabad, Telangana, India.*
[2]*Department of Humanities and Sciences, Vidya Jyothi Institute of Technology, Hyderabad, Telangana, India.*
[3]*Department of Chemistry, Nizam College, Basheerbagh, Osmania University, Hyderabad, Telangana, India.*
[4]*Department of Chemistry, University College of Science, Saifabad, Osmania University, Hyderabad, Telangana, India.*

ARTICLE INFO

Article history:
Received: 24 January, 2024
Revised: 05 May, 2024
Accepted: 16 May, 2024
Published: 30 May, 2024

Keywords:
NuoC protein, Protein 3D modeling, Protein validation, Molecular dynamics, Active site prediction, Virtual screening, MM/GBSA calculations, ADME analysis.

DOI:
10.25004/IJPSDR.2024.160302

ABSTRACT

One of the most serious medical conditions is tuberculosis (TB). In *Mycobacterium tuberculosis* (Mtb), the NADH-quinone oxidoreductase subunit C (NuoC) protein is a member of the NADH dehydrogenase family and is essential to the electron transport chain, ATP generation, and energy production. One possible pharmacological target for finding inhibitors is the Nuoc protein. Computational approaches are used to identify the 3D structural characteristics of the Nuoc protein, and several validation methods are used to verify the results. Using several ligand databases, virtual screening tests surrounding the active site were carried out to find drug-like molecules. The study found that the amino acid residues that are important in drug-target interactions are ARG98, ARG75 (basic), ASP99, ASP189, ASP98 (acidic), LEU101, LEU194 (nonpolar neutral), THR180 (polar neutral), GLU177 (polar neutral), TYR181 (polar neutral), PRO102, PRO192 (nonpolar neutral), and HIS191 (basic). The findings demonstrate the ligand molecules' drug-like ability to inhibit NuoC proteins. The structural data may be used to develop novel therapeutic scaffolds for the treatment of tuberculosis (TB), in conjunction with information on the active site and the chosen ligand molecules.

INTRODUCTION

Millions of people around the world are affected each year by tuberculosis (TB),[1,2] the second largest cause of death.[3,4] An intracellular pathogenic bacterium called *Mycobacterium tuberculosis* (Mtb)[5] is the source of this deadly illness. In the report on TB released in 2023,[6,7]the World Health Organisation (WHO) stated that approximately 7.5 million people will be newly diagnosed with TB in 2022. Currently, several medications, including the BCG vaccine [8,9], are provided; these medications can be categorized as first- or second-line treatments.[10] Isoniazid, rifampicin, ethambutol, and pyrazinamide are essential first-line treatments. For second-line therapies, "Ethionamide, Para-aminosalicylic acid, Cycloserine, Ofloxacin, Amikacin, and Ciprofloxacin" were considered.[11-13] Increasing medication resistance in Mtb strains is the main issue with TB therapy.[14] The treatment of drug-resistant tuberculosis (DR-TB), employs DOTS plus therapy[15,16] which has several adverse effects. Failure to respond to TB therapy is caused by mutations in the Mtb gene.[17] Scientists in the field of TB drug discovery are now working to create innovative treatments that address TB.[18, 19]

***Corresponding Author:** Dr. Vasavi Malkhed

Address: Department of Chemistry, University College of Science, Saifabad, Osmania University, Hyderabad, Telangana, India.

Email ✉**:** mvasavi@osmania.ac.in

Tel.: +91-9866929299

Relevant conflicts of interest/financial disclosures: The authors declare that the research was conducted in the absence of any commercial or financial relationships that could be construed as a potential conflict of interest.

The Mycobacterium have evolved to live in a range of settings, including both inside and outside of cells. These bacteria need oxygen to exist. Their capacity to use a variety of energy sources and to go on with metabolic activities even when they are not actively developing are two important aspects of this adaptability. Because Mtb is an obligate aerobic heterotroph, it cannot grow or survive without oxidative phosphorylation. Alternative electron donors and acceptors play a crucial role in providing the energy required for a bacterium to exist in hypoxic, non-replicating states when it comes to latent infections. These other energy sources are essential for pathogen persistence and possible reactivation, which adds to the difficulty of treating latent infections. Developing tailored therapeutics to combat latent infections can benefit greatly from an understanding of the mechanisms by which bacteria use alternate electron donors and acceptors [20]. Oxidative phosphorylation and respiration depend on the NDH-I protein complex. The respiratory chain's entrance site for electrons is the NDH-I complex. It is composed of 14 subunits in Mtb that are encoded by the nuo operon. NuoAHJKLMN genes encode seven subunits that penetrate the lipid bilayer. The peripheral subunits are encoded by a different set of seven nuo genes.[21,22]

The NDH-I complex proteins greatly influence the way that Mtb reacts to nitrosative stress. Nitric oxide (NO), which is produced by the inducible nitric oxide synthase (iNOS) in Mtb-infected macrophages, is one of the reactive nitrogen species (RNS) released by the host in response to Mtb infection of human cells. Even though it is deadly, Mtb has developed defenses against RNS. Scavenging, iron sequestration, inhibiting the synthesis of RNS, and catalytic detoxification are some of these methods. One of the elements of Mtb's defense mechanism against nitrosative stress is the Nuoc protein.[23]

The NADH-quinone oxidoreductase subunit C (NuoC) protein is one of the peripheral proteins of the NDH-I complex.[24,25] It is essential for the Mtb electron transport chain, ATP generation, and energy production. Thus, targeting the NuoC protein to discover new leads will help in the discovery of new TB antibiotics, and it is safe to target NDH-I class proteins as these proteins are absent in humans.

Materials And Methods

One of the conventional approaches to drug design is the random screening of substances synthesized in laboratories or found in nature. The exorbitant cost and protracted design cycle of this technology are among its drawbacks. The introduction of informatics, computational approaches, and structure-based drug design (SBDD), among other current strategies, has greatly sped up the drug development process.[26-28] Thus, the NuoC protein theoretical model is generated and validated.

Model Generation

SBDD requires knowledge about the three-dimensional (3D) structure of the target protein. In the absence of a structure generated experimentally, a hypothetical 3D structure is generated using homology modeling [29-31].

The sequence (Primary) of the NuoC protein (amino acids) is procured in FASTA format for homology modeling from the proteomic servers ExPASy (Expert Protein Analysis System) and Universal Protein Resource (UniProtKB).[32-34] The identified proteins with similar fold similarity, domains, and secondary structure serve as templates using the server programs Phyre 2,[35] JPred4,[36] and BLAST.[37] The BLAST program facilitated the identification of the most approximate template for the target, employing Karlin and Altschul's (1990) stochastic model. The similarity between the target and template was quantified by the expectation value (E-value), which considers sequence conservation. The target protein sequence was aligned with the template amino acid sequences using the CLUSTALW software. Following this, a 3D model of the NuoC protein was created using MODELLER 10.2v and the CHARMM22 force field. This process involved molecular modeling and energy minimization to accurately represent the 3D structure of the protein.[38] The protein model with the lowest MODELLER objective function was selected for further optimization processes with CHARMM22 force field.[39,40] The NuoF protein 3D model is chosen for additional optimization processes.

Optimization and Validation of the 3D Model

The models produced by MODELLER 10.2v were checked for stereochemical quality using the PDBsum server's Ramachandran plot.[41,42] Energy minimization comes next, with the quality of the prioritized 3D model being improved by the molecular dynamics simulations from the locPREFMD server.[43,44] The Schrödinger suite's Autoprep module uses the optimised potentials for liquid simulations (OPLS) 2003 force field[45] to maintain the native conformation of the carbon chain backbone in the protein structure while reducing model energy. The cut-off root mean square deviation (RMSD)[46] of the model is set to 0.3. Without modifying the protein's C-chain coordinates, the Autoprep module precisely preserves the side chain positions while permitting the backbone amino acids to continue being moveable in order to achieve a workable lowest energy state conformation. The ProSA server[47] was used to ascertain the general and local model quality. The PDBsum server provides the target protein's secondary structure. To evaluate the accuracy of the created homology model of the NuoC protein, RMSD analysis between the templates and the target is performed, and the total energy of the protein is determined using the SPDBV 4.0 program [48].

Active Site Identification by In-silico Methods

Finding a protein's active site is essential for drug discovery since it helps us understand the precise biological function of the protein. Finding the regions of the protein most likely to have binding sites is done computationally. Hydrophobic areas are predicted using the CASTp tool[49–51] allosteric regions were predicted by the Schrödinger suite's SiteMap module.[52,53]

Docking and Virtual Screening

The Schrödinger suite's Glide module[54,55] is employed to build a grid for the purpose of examining the NuoC protein's binding domain. Docking experiments and virtual screening[56-59] are performed using ligands chosen from structural databases. To maximise the ligands' stereochemistry, ionisation states, and ring conformations prior to the virtual screening, the LigPrep module[60,61] from the Schrödinger suite is employed. The virtual screening process used by the Glide program for docking consists of the HTVS[62], SP, and XP modes.[63] The Glide score is assigned to each docked ligand in order to ascertain the affinity. The outcomes of virtual screening studies were further analyzed.

MM/GBSA Calculations

The ΔG_{Bind} values[64] of small molecular ligands that are acquired as a result of XP docking are calculated by the "Prime Generalised Born Surface Area (MM/GBSA)" module[65,66] of the Schrödinger suite. The following formula can be used to calculate $\Delta G_{Bind.}$

$\Delta G_{(Bind)} = \Delta E_{(MM)} + \Delta G_{(GB)} + \Delta G_{(SA)} - T\Delta S$

$\Delta EMM = \Delta E internal + \Delta E electrostatic + \Delta Evdw$

In the generalized born (GB) model, the electrostatic solvation energy is represented by the equation $\Delta G_{(GB)}$. On the other hand, in the solvent accessible surface area (SASA) model, the non-electrostatic solvation component is represented by $\Delta G_{(SA)}$. Standard molecular dynamics simulations are used to determine the change in conformational entropy, which is represented by the value of -TΔS.

ΔG_{Bind} = ΔE complex (minimised) - [ΔE ligand (unbound, minimized) + ΔE receptor (unbound, minimized)]

The strain energies of the ligand and receptor rings are considered in the relative free energy (ΔG_{Bind}). To compute, Prime uses the following: ΔE ligand (unbound, minimized) for the free ligand's MM/GBSA following its extraction from the protein-ligand complex; ΔE receptor (unbound, minimized) for the protein's MM/GBSA upon its dissociation from the ligand; and ΔE complex (minimized) for the energy-minimized complex.

ADME Properties

Before initiating clinical trials and bringing lead molecules to market, it is vital to thoroughly evaluate the ADME properties of drug-like molecules.[67-69] The absorption, distribution, metabolism, and Excretion (ADME) properties of the newly discovered ligand structures were thoroughly analyzed using the QikProp module, a part of the comprehensive Schrödinger suite. This module assists in the prediction and evaluation of various pharmaceutical properties such as solubility, permeability, and metabolic stability, providing valuable insights into the potential behavior of the ligands within biological systems.[70] The ligand structures with promising potential as effective treatment candidates for TB were selected based on the favorable projected values of absorption, distribution, metabolism, and elimination.

Molecular Dynamics Simulation Analysis

The OPLS-2005 force field was utilized to process the force field and generate the topology for the L1-NuoC complex molecular dynamics simulation, which was performed using Desmond 2021-4.[71,72] Using the system builder platform, the complex was created by solving the orthorhombic simulation box's simple point-charge (SPC) explicit water model. To replicate physiological circumstances, the solvated complex system was neutralized using a concentration of 0.15 M salt and an appropriate quantity of Na^+ /Cl^- counter ions. The receptor-ligand complex system was identified using the OPLS-2005 force field, and an explicit solvent model including SPC water molecules was used in an orthorhombic box. After 100 picoseconds of Desmond reduction, the system was relaxed using the BioLuminate default technique. The next procedure was followed by simulations, which ran for 100 nanoseconds at 300 Kelvin and 1.0325 bar of pressure.

RESULTS AND DISCUSSION

Structural Evaluation of NuoC Protein

A potential new therapeutic target for TB is the 236 amino acids long NuoC protein. Homologous proteins were found to be suitable templates for constructing its 3D model. Their domain similarities, secondary structure, and sequence with the NuoC protein sequence were examined to achieve this. Template search was conducted using tools like Phyre 2, JPred4, and BLAST. The template search program PSI-BLAST was used to find templates with amino acid sequences similar to the NuoC protein. A strong biological link between the NuoC protein amino acid sequence (Table 1) is indicated by the low expect value of 3MCR_A.

Templates having an amino acid sequence similar to the NuoC protein can be located using the BLAST. The program BLAST uses Karlin and Altschul's (1990) stochastic model to identify a template that most closely matches the target. The 3MCR_A amino acid sequence's low E-value points to a highly relevant biological relationship.

Table 1: Template search for NuoC protein

S. No	*Tool for searching templates*	*%identity*	*Expect value/percentage of confidence*	*PDB code of template procured*
1.	PSI BLAST	53.55	2e-73	3MCR_A
2.	JPred4	-	2e-59	3MCR_A
3.	Phyre 2	63	100	3MCR_A

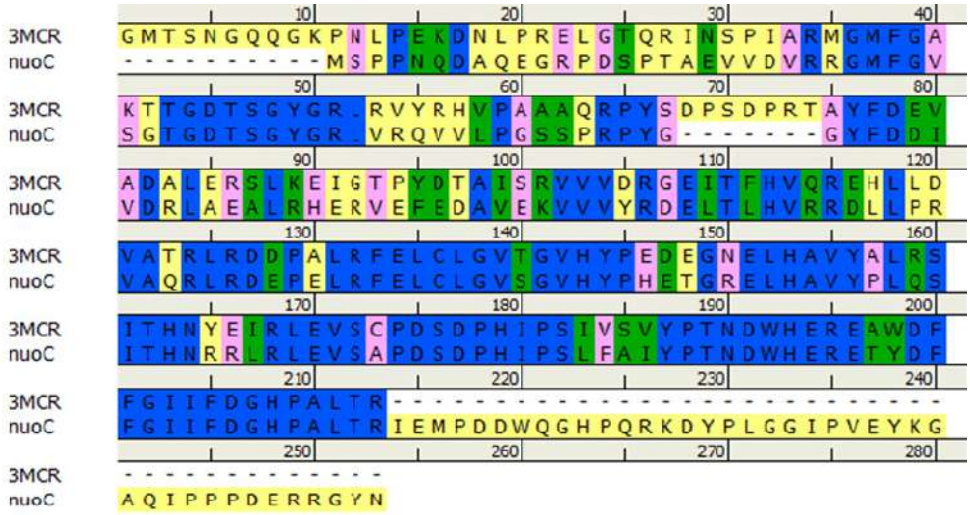

Fig. 1: shows the alignment of NuoC with the 3MCR_A protein sequence. The color blue denotes identical residues, green denotes very similar residues, pink denotes weakly similar residues, and yellow denotes non-matching residues

The JPred4 algorithm utilizes a comprehensive approach to identify template proteins with closely resembling secondary structures by employing a diverse set of sequence alignment profiles. JPred4 harnesses the JNet method to accurately forecast the occurrence of specific secondary structure elements in proteins, such as helices, sheets, and loops. Notably, with an impressively low E-value of 2e-59, JPred4 strongly recommends utilizing chain "A" of template 3MCR for the given protein analysis. Using statistics like %of identity and %confidence, one can determine the extent to which the sequence is preserved relative to the structure. The Phyre 2 server's confidence value (Table 1) indicates the likelihood that the target and template amino acid sequences will be similar. The 3MCR_A template demonstrates 63% identity and 100% confidence (Fig. 1). The best template for homology modeling of NuoC protein appears to be 3MCR_A, according to all three template search tools.

The method for identifying correlations between two amino acid sequences of proteins that may indicate functional, structural, or evolutionary connections is called pairwise sequence alignment, or PSA. The CLUSTALW web server achieved the PSA of the template 3MCR_A and NuoC. An alignment score of 50.70 is obtained, indicating appreciable similarity between template and target. The generated alignment file is visualized using Discovery Studio Visualiser (Fig. 1) and further used in homology modeling by MODELLER software.

Accurate three-dimensional structures can be obtained by aligning phylogenetically related template proteins with the NuoC protein sequence. The MODELLER 10.2v software was utilized to construct the 3D structure, employing the alignment file (Fig. 1), the 3D coordinates file of the template, and the FASTA sequence of the NuoC protein. Subsequently, the model characterized by the lowest Modeller goal function was chosen for further investigation. Molecular dynamics improved the model's quality in the locPREFMD server (Table 2). The application of molecular dynamics resulted in a significant enhancement in the stability characteristics of the NuoC protein's 3D structure which is confirmed with energy calculations from SPDBV 4.1.0 software. The energy of conformations before and after dynamics is calculated. Energy was found to have decreased from 1376.452 to -7616.292 kJ/mol. The results indicate that the NuoC dynamically stabilized.

Validation of Theoretical Structure of NuoC Protein

The Ramachandran contour plot, shown in Fig. 2 and Table 3, is a fundamental visual tool used to analyze and assess the stereochemical quality of protein structures. It provides a graphical representation of the backbone dihedral angles of amino acid residues in proteins, aiding in the identification of favorable and unfavorable conformations. According to plot results, 92.1% of the residues in the protein that was homology-modelled are located in the most advantageous energy landscapes.

Table 2: List of NuoC protein stabilization variables after molecular dynamics

S. No	*Variables examined*	*Before dynamics*	*After dynamics*	*Goal*
1	phi-psi backbone favored region	92.70	92.10	>90%
2	phi-psi backbone allowed region	6.800	7.300	
3	phi-psi backbone general region	0.500	0.500	<1%
4	phi-psi backbone disfavoured region	0.000	0.000	<0.2%
5	chi 1-chi2 side chain unallowed region	0.021	0.021	<0.2%
6	G-factor covalent bonds	0.020	0.050	> -0.5
7	G-factor overall interactions	-0.220	-0.180	> -0.5
8	Favorable main-chain bond lengths	100.00	100.0	100%
9	Favorable main-chain angles	90.90	91.80	100%
10	Sidechain ring planarity	99.10	99.10	100%

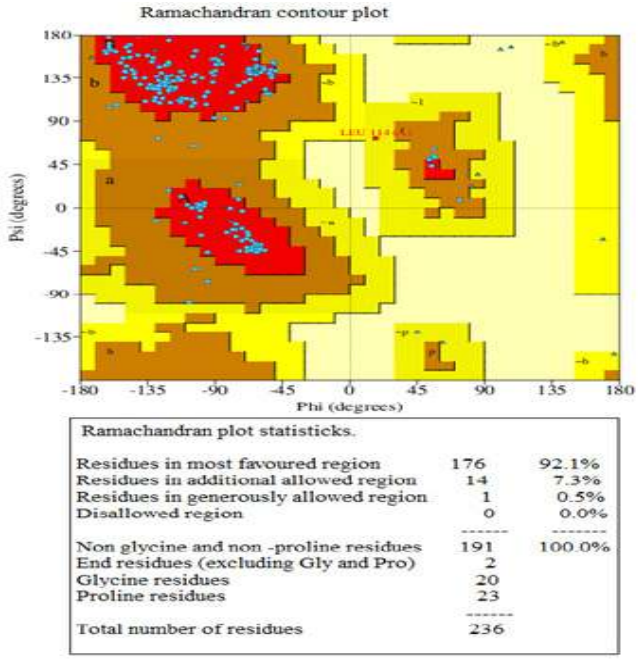

Fig. 2: The NuoC protein's Ramachandran plot. There are four regions in the NuoC protein's Ramachandran plot. The plot's red-colored field denotes the location that is energetically most preferred. The areas that are further permitted are shown by the brownfield, the liberally permitted areas by the yellow field, and the prohibited areas by the light-yellow field. The majority of the NuoC protein's 236 amino acid residues, specifically 176 residues, are positioned within the energetically most preferred region. This observation indicates that the protein structure exhibits a high level of stereochemical quality

Given its superior stereochemical quality, the homology-modelled protein is considered for additional validation. The ProSA energy plots are also used to evaluate the NuoC protein structure. The Z-score (-3.61) of the NuoC protein falls within the range of similar-sized proteins whose structures have been determined by NMR spectroscopy (shown in dark blue) or X-ray crystallography (shown in light blue). This points to a very high degree of overall model quality.

Knowledge-based energy values are used in the ProSA energy profile to provide local model quality. The energy map in Fig. 3 has two sections with window widths of 10 and 40 amino acids. The low energy profile graphs show that the three-dimensional structure of the NuoC protein is reliable.

Secondary Structure Prediction of NuoC Protein

The stability and conformation of proteins depend on their secondary structures. Utilizing the PDBsum create server, the secondary structural data for the NuoC protein[73] is deduced. It provides information in the form of pictures. NuoC contains one beta-sheet, five beta strands, and six helices, as per the results (Table 4). Three helix-helix interactions further stabilise NuoC protein (Table 5, Fig. 4).

Conserved Domain Analysis and Active Site Identification of NuoC Protein

Proteins in the NADH dehydrogenase family are highly conserved. The information regarding the various NuoC protein conserved domains that were found through BLAST is displayed in Fig. 5 CASTp and Schrödinger's SiteMap module were used to anticipate the NuoC protein active site zones. Two potential active site areas (site 1 and site 2) were shown by the SiteMap and two probable active site locations (pocket1 and pocket2) were shown by the CASTp server (Table 6). Strong support for the active site anticipated by the literature is provided by residues 46–154 in the SiteMap and residues 82–154 in CASTp.

Docking and Virtual Screening Studies of NuoC Protein

The ligands and proteins from the Bionet ligand database were prepared using LegPrep and the Protein Preparation Wizard, respectively. A Grid measuring 80Å×80Å×80Å was created, incorporating residues from the active site of ATP binding. After being virtually screened with NuoC, the produced ligands were sent through the QikProp filter. Out of the 39, 490 ligands that underwent virtual screening with the HTVS, SP, and XP modes, LigPrep generated 79,430 molecules. The end product produced sixty molecules, of which the best eight (L1-L8) were subjected to additional analysis using Glide energy and Glide score.

Table 3: Ramachandran plot statistics

Regions in the RC plot	*Number of residues*	*percentage*
Most desirable region	176	92.1
extended desirable region	14	7.3
Generously desirable region	1	0.5
Disallowed regions	0	0.0
Residues other than glycine and proline	191	100
Terminal residues (excluding Gly and pro)	2	-
Number of glycines	20	-
Number of prolines	23	-
Total number of amino acid residues	236	-

Knowing the ligand-biological target interactions requires an understanding of the ligand pharmacophores. Because the ligands from L1 to L8 have different pharmacophores, they bound to different amino acids but at the active site region. Piperazine from L2, piperazine and piperidine from L8, N-methyl piperidine-4-amine from L5, N, N-diethylethane-1,2-diamine from L4, pyrrolidine from L7, N-methyl-2-oxidanylethane-1-amine from L6, phenyl methionamine from L1, (E)-N, N, N-trimethyl formamide and piperazine from L3 are the groups functioning as pharmacophores. The amino acid residues ARG98, ARG75 (BASIC), ASP99, ASP189, ASP98 (acidic), LEU101, LEU194 (nonpolar neutral), THR180 (polar neutral), GLU177 (polar neutral), TYR181 (polar neutral), PRO102, PRO192 (nonpolar neutral), and HIE191 (basic) are consistently interacted by all the ligands from L1-L8. The aforementioned characteristics of ligands and interacting amino acid residues clearly show the affinity with NuoC protein (Table 7), (Table 1,2 supplementary).

Table 4: Secondary structural information of NuoC protein

		Helices		
S. No	*Starting residue*	*Ending residue*	*No of residues*	*Sequence*
1.	Gly58	Arg72	15	GYFDDIVDRLAEALR
2.	Glu77	Asp80	4	EFED
3.	Leu100	Arg109	10	LLPRVAQRLR
4.	Asp174	Asp182	9	DWHERETYD
		Beta strands		
1.	Ala81	Val85	5	AVEKV
2.	Leu92	His95	4	LTLH
3.	Glu117	Val125	9	ELCLGVSGV
4.	Glu134	Leu141	8	ELHAVYPL
5.	Leu150	Ser155	6	LRLEVS
		Beta Sheet		
Sheet		No of stands		Type
A		5		Mixed

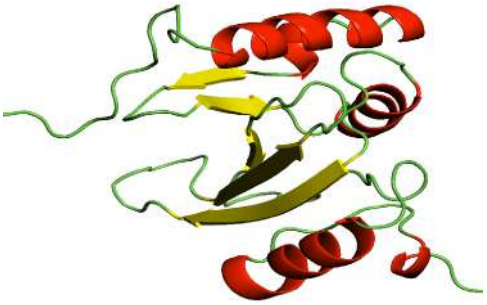

Fig. 4: shows the secondary structure of NuoC in pictorial form. 3D form of NuoC protein, represented as helices in red, sheets in yellow, and loops in green color, respectively

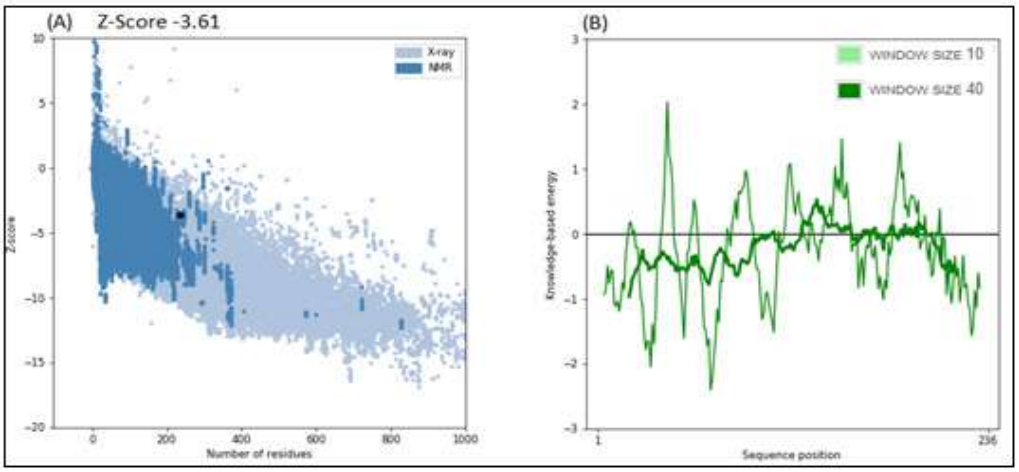

Fig. 3: shows (A) an overall model quality plot of the Z-score against the number of residues. Structures deposited using X-ray and NMR techniques are indicated by light blue and dark blue colors, respectively. A Z-score of -3.61 for NuoC indicates that the structure is very reliable. (B) The knowledge-based energy against the sequence position plot shows the quality of the local model

Table 5: List of helix-helix interactions

Interactions between helices			
S. No	*Interactions between helices*	*Distance (Å)*	*Count of interacting residues*
1	A1-A2	8.1	6
2	A1-A4	10.5	7
3	A2-A4	9.8	1

MM/GBSA Calculations

Ligands are rated and assessed according to the extent of their affinity for biological targets when computational methods develop pharmaceuticals. The affinity between ligand and biological target can be predicted by MM/GBSA simulations (Table 8). The ΔG_{Bind} values emphasize the biological target's affinity for the ligand; the higher the affinity, the more negative the values. The thermodynamic viability of complexation is illustrated by the rise in the free energy value of ligands upon complexing with biological targets. The ligands L1, L2, L3, L4, L5, L6, L7, and L8 exhibit spontaneity in complexation with NuoC protein as evidenced by a decrease in free energy.

ADME Analysis

Since many drugs and lead compounds fail at a late stage of pharmaceutical development due to unfavorable pharmacokinetic properties, predicting ADME qualities is crucial throughout the lead compound selection process. A mathematical representation of a structural or physicochemical characteristic of a molecule or a portion of a molecule is called a molecular descriptor. To look into the ADME characteristics of possible leads, a variety of pertinent molecular characteristics, or descriptors, are frequently employed. An attempt has been made to assess the ligands' ADMET profiles in *in-silico*. Out of the 46 descriptors generated by Schrodinger's QikProp, only 13 were taken into consideration (Table 9).

Descriptors for lead substances include molecular weight, hydrogen bonds, and QPlogS, which indicate aqueous solubility. For absorption, high values are >80% and low values are 25%. Caco-2 cells determine the permeability of the gut-blood barrier, and the CNS ranges from inactive to active. The Rule of five requires "MW <500, QPlogPo/w <5, donorHB ≤5, and accptHB ≤10" for drug-like substances. QPlog Po/w predicts how drugs interact with real membranes.

The molecular weight of ligands from L1 to L8 are 291.39-420.55, QPlogPo/w ranges from 0.649- 4.614, donor HB 1 to 4 and, acceptor HB 3-9 accepting the Rule of five. The QplogS values of L1-L8 are within the acceptable value, that is, from -4.89 to -0.534. The ligands L3, L4, L7 and L8 show %HOA >80 % suitable for oral drugs. The Caco-2 values of all the ligands are greater than 25, reflecting good permeability for the gut-blood barrier. The CNS values of all the ligands except L4 and L8 show inactivity (values 0 and 1) towards CNS. The QPlog Khsa values, which represent human serum albumin binding, are within the range of -0.291 to 0.394. The QPlogBB and QPlog HERG, which represent blood blood-brain barrier and Ic_{50} values for HERG K+ channels, respectively, show permissible ranges of molecular descriptor values. The aforementioned ADME values of ligands will help in the selection of the most compatible inhibitor for the NuoC protein.

MD Simulation Results for L1-NuoC Complex

During the study, a molecular dynamics (MD) simulation lasting 100 nanoseconds was conducted for the top-docked compound L1. The primary objective of the MD simulations was to evaluate the stability of the interactions between the ligand-protein docked complexes. Specifically, the focus was on investigating the stability of the protein (NuoC) in conjunction with the L1 ligand at the respective binding site. This investigation involved performing an RMSD analysis of the protein backbone of the initial frame structure. The RMSD value of protein was found to be stable between 20.8 to 24 Å from a 45 to 100 ns time frame after a 1 to 10 ns time frame trajectory tried to get the equilibrium stage and showed fluctuation between 10 to 45 ns time frame. The ligand RMSD followed the protein RMSD till 40 ns after that, tried to be stable between 15 to 21 Å from a 40 to 100 ns time frame and showed fluctuation between 10 to 45 ns time frame (Fig. 6). The RMSF plots of protein (side chains) and ligand showed protein residue that interacts with the ligand

Table 6: Identification of active site

S. No	*Active site prediction tool*	*Pocket and Site numbers*	*Volume Å^3*	*Amino acids*
1	CASTp	1	48.904	VAL82, GLU83, LEU94, HIS95, THR131, GLY132, LEU152, VAL154.
2		2	40.139	VAL46, VAL47, LEU48, GLY50, GLU83, VAL85, LEU92, LEU94, HIS126, HIS129, LEU135, LEU152, VAL154
3	SiteMap	1	121.765	VAL46, VAL47, LEU48, GLU83, VAL85, LEU92, LEU94, HIS129, LEU135, LEU152, VAL154
4		2	84.035	ILE63, ARG66, LEU67, ALA70, GLU77, PHE78, ASP80, ALA81, VAL82, GLU83, LYS84, ARG103

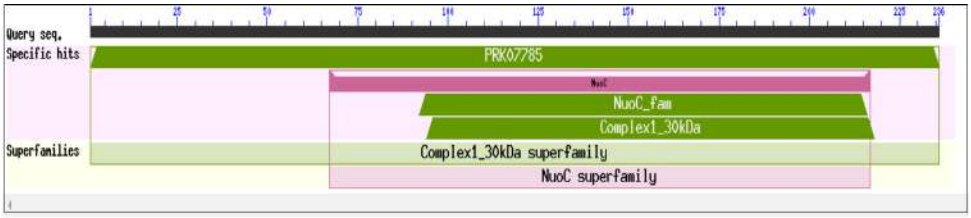

Fig. 5: shows a pictorial representation of conserved domains of the NADH dehydrogenase family

Table 7: List of ligands having an affinity with NuoC protein

Ligand number	*Glide score*	*Glide energy*
L1	-7.305	-43.06
L2	-7.127	-42.08
L3	-7.192	-7.121
L4	-7.121	-35.62
L5	-6.895	-29.19
L6	-6.875	-35.65
L7	-6.290	-48.30
L8	-6.253	-36.22

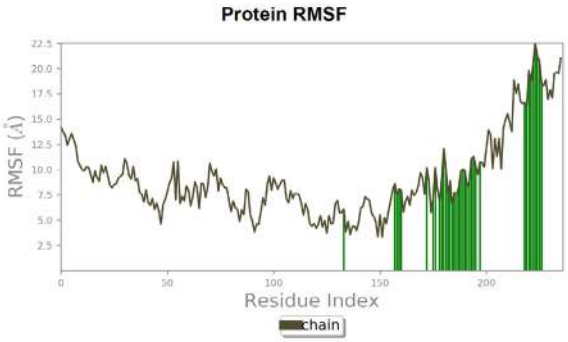

Fig. 7: The plot of protein side chains' root mean square fluctation (RMSF) (NuoC)

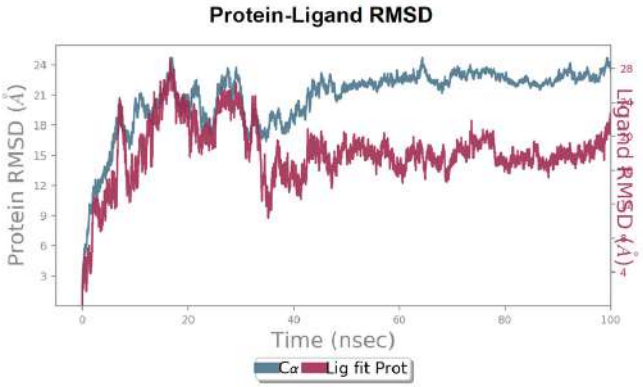

Fig. 6: The protein NuoC and ligand L1's root mean square deviation (RMSD) during 100 ns of MD simulation is displayed on the graph

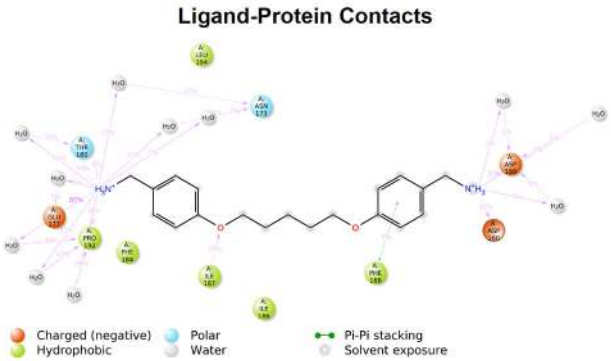

Fig. 8: Binding interactions of ligand L1 with NuoC during MD Simulation of 100 ns

Table 8: MM/GBSA calculations of ligands

Ligand number	*Free energy of ligand*	ΔG_{Bind}	ΔG_{Bind} *Coloumb*	ΔG_{Bind} *Covalent*	ΔG_{Bind} *solvent*	ΔG_{Bind} *vdw*
L1	-22.598	-35.072	-105.536	3.282	110.124	-26.749
L2	68.602	-28.202	-74.671	9.173	74.682	-21.381
L3	18.786	-27.081	-102.110	5.159	100.042	-15.7262
L4	19.114	-39.446	-75.362	-2.156	75.799	-21.105
L5	8.422	-33.692	-72.514	1.884	74.888	-21.2803
L6	58.092	-30.973	-109.738	1.971	101.601	-15.121
L7	23.842	-41.398	-83.120	4.551	88.262	-31.962
L8	47.381	-39.191	-71.675	3.368	68.900	-25.805

Table 9: ADME properties of most compatible ligands

Ligand number	*Physico-chemical properties*				*Pharmaco-kinetic properties*							*Drug-likeness properties*	
	MW	*DHB*	*AHB*	*QP logs aqueous solubility*	*% HOA*	*QPP Caco*	*QPLOG Khsa*	*QPlog Po/w*	*QPlogBB*	*CNS*	*QPlog HERG (PLC50)*	*Rule of five*	*Rule of three*
L1	314.42	4	3.5	-1.993	71.981	42.027	0.208	2.729	-0.65	0	-7.555	0	1
L2	335.42	2	9	-0.989	56.502	27.482	-0.163	0.649	0.436	1	-7.389	0	0
L3	406.83	1	7.5	-4.89	95.859	500.15	0.236	3.519	0.311	1	-5.933	0	0
L4	381.34	2	4.2	-3.748	100	316.81	0.64	4.614	0.793	2	-7.344	0	0
L5	291.39	3	5	-2.205	67.149	41.151	0.156	1.931	-0.345	0	-7.127	0	0
L6	312.25	4	3	-0.534	72.59	76.057	-0.291	2.045	0.38	1	-4.922	0	0
L7	420.55	2	9	-4.176	81.255	100.15	0.394	3.16	-0.106	1	-8.239	0	0
L8	334.43	1	7.5	-2.67	81.674	225.15	0.111	2.156	0.77	2	-6.664	0	0

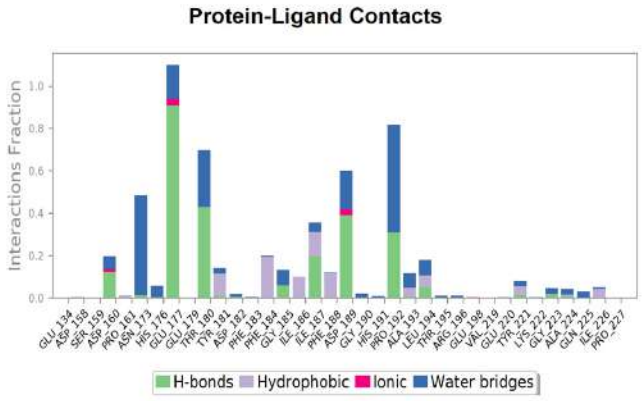

Fig. 9: Interaction fraction of various residues (L1-NuoC complex)

between 4 to 14 Å, respectively, protein-ligand interaction was showed by green-colored vertical bars (Fig. 7). The 100 ns trajectory was analyzed to study the interactions. During this period, specific amino acid residues such as Glu177, Pro192, Asp160, Asp189, Thr180, and Ile187 were found to be involved in hydrogen bond interactions (both backbone and sidechain) with the protein. Additionally, Tyr181, Phe184, and Ile186 were observed to participate in hydrophobic interactions with the protein, while Phe188 was found to be involved in π-π interactions with the protein, as shown in Fig. 8. The interaction fraction of different amino acid residues has been detailed in Fig. 9 [74].

Conclusion

The 236 amino acid NuoC protein is a viable biological target for the creation of antibiotics that target Mtb. A theoretical model of the NuoC protein was created using the homology modeling approach, and it was then improved by doing molecular dynamics simulations. The model's integrity was rigorously assessed using the Ramachandran plot and ProSA energy plots. Through the utilization of in-silico tools, the active site, spanning from amino acid residues 46 to 154, was predicted. Subsequent docking and virtual screening procedures were executed within the predicted active site region. The screened ligand molecules exhibited distinct pharmacophores, with ligands L1-L8 demonstrating negative values of ΔGBind, affirming the thermodynamic feasibility of the protein-ligand complex formation. Furthermore, the ADME values of ligands L1-L8 were found to be within permissible ranges. Notably, molecular dynamics studies of the top-scored ligand L1 with the NuoC protein revealed substantial stability of the L1-NuoC complex. The results emphasize the significant potential of the anticipated NuoC protein inhibitors in aiding the creation of innovative drugs aimed at treating tuberculosis.

Acknowledgement

The authors, HRB, LR, MB, and RM, extend their sincere appreciation to the Principal and the Head of the Department of Chemistry, University College of Science, Osmania University (O.U.), for generously providing the necessary facilities for conducting our research work. Furthermore, we would like to express our gratitude to the Department of Chemistry, University College of Science, O.U., Hyderabad, for the exceptional facilities made available through the DST-FIST and UGC-UPE support. Our acknowledgment also extends to the facilities established by DST-FIST at the Department of Chemistry, UCS, Saifabad, O.U., Hyderabad.

References

1. Mejbel FAH, Aljanaby IAJ, Al Hadrawi KK, Aljanaby AAJ. Pulmonary Tuberculosis Risks and Challenges. In the proceedings of the 2023 E3S Web Conference. 2023, pp. 381 (April). Available from: doi.org/10.1051/e3sconf/202338101101.
2. Lee BS, Pethe K. Telacebec: An Investigational Antibacterial for the Treatment of Tuberculosis (TB). Expert Opin. Investig. Drugs. 2022;31(2):139–144. Available from: doi.org/10.1080/13543784.2022.2030309.
3. Sandhu G, Tuberculosis: Current Situation, Challenges and Overview of Its Control Programs in India. J. Glob. Infect. Dis. 2011;3(2):143–150. Available from: doi.org/10.4103/0974-777X.81691.

4. Villar-Hernández R, Ghodousi A, Konstantynovska O, Duarte R, Lange C, Raviglione M. Tuberculosis: Current Challenges and Beyond. Breathe. 2023;19(1):3–7. Available from: doi.org/10.1183/20734735.0166-2022.
5. Ifijen IH, Atoe B, Ekun RO, Ighodaro A, Odiachi IJ. Treatments of Mycobacterium Tuberculosis and Toxoplasma Gondii with Selenium Nanoparticles. Bionanoscience 2023; 13(1):249–277. Available from: doi.org/10.1007/s12668-023-01059-4.
6. World Malaria Report 2023; 2023. Available from: https://www.who.int/teams/global-malaria-programme/reports/world-malaria-report-2023
7. Global Tuberculosis ReporT 2022; 2022. Available from: http://apps.who.int/bookorders.
8. Wang PH, Lin SY, Liou HH, Chen CC, Shu CC, Lee CY, Tsai MK, Yu CJ. Protective Effect of BCG and Neutrophil-to-Lymphocyte Ratio on Latent Tuberculosis in End Stage Renal Disease. Infect. Dis. Ther. 2023;12(7):1907–1920. Available from: doi.org/10.1007/s40121-023-00839-5.
9. Korotetskaya M, Baikuzina P, Apt A. Inability of the BCG Vaccine to Protect Mice of the H2f Haplotype at Advanced Stages of TB Infection Is Associated with Defective CD4+ T-Cell Activation in Spleen. Tuberculosis 2023;143:102429. Available from: doi.org/10.1016/j.tube.2023.102429.
10. Wu C, Yi H, Hu Y, Luo D, Tang Z, Wen X, Zhang Y, Tang M, Zhang L, Wu S, Chen M. Effects of Second-Line Anti-Tuberculosis Drugs on the Intestinal Microbiota of Patients with Rifampicin-Resistant Tuberculosis. Front. Cell. Infect. Microbiol. 2023;13 (April):1–12. Available from: doi.org/10.3389/fcimb.2023.1127916.
11. Arushothy R, Jamaludin FN, Samsudin N, Yong KL, Hashim R. Characterization of Non-Vaccine Type Streptococcus Pneumoniae in Malaysia. Int. J. Infect. Dis. 2023;130:S88–S89. Available from: doi.org/10.1016/j.ijid.2023.04.220.
12. Van Schalkwyk M, Bekker A, Decloedt E, Wang J, Theron GB, Cotton MF, Eke AC, Cressey TR, Shapiro DE, Bacon K, Knowles K, George K, Browning R, Chakhtoura N, Rungruengthanakit K, Wiesner L, Capparelli EV, Stek AM, Mirochnick M, Best BM. Pharmacokinetics and Safety of First-Line Tuberculosis Drugs Rifampin, Isoniazid, Ethambutol, and Pyrazinamide during Pregnancy and Postpartum: Results from IMPAACT P1026s. Antimicrob. Agents Chemother. 2023;67(11):1–18. Available from: doi.org/10.1128/aac.00737-23.
13. Sathiyamoorthi S, Pentapati SSK, Vullanki SS, Avula VCR, Aravindakshan R. A Case of Delusional Disorder With Abuse of Isoniazid, Rifampicin, Pyrazinamide, and Ethambutol, the First-Line Anti-tuberculosis Therapy Drugs in India. Cureus. 2023 Mar 29;15(3):e36893. Available from: doi: 10.7759/cureus.36893.
14. Palomino, J. C, Martin, A.Drug Resistance Mechanisms in Mycobacterium Tuberculosis. Antibiotics. 2014;3(3):317–340. Available from: doi.org/10.3390/antibiotics3030317.
15. Ramanathan K, Antognini D, Combes A, Paden M, Zakhary B, Ogino M, MacLaren G, Brodie D, Shekar K. Planning and provision of ECMO services for severe ARDS during the COVID-19 pandemic and other outbreaks of emerging infectious diseases. Lancet Respir Med. 2020 May;8(5):518-526. Available from: doi: 10.1016/S2213-2600(20)30121-1.
16. Merker M, Rasigade JP, Barbier M, Cox H, Feuerriegel S, Kohl TA, Shitikov E, Klaos K, Gaudin C, Antoine R, Diel R, Borrell S, Gagneux S, Nikolayevskyy V, Andres S, Crudu V, Supply P, Niemann S, Wirth T. Transcontinental spread and evolution of Mycobacterium tuberculosis W148 European/Russian clade toward extensively drug resistant tuberculosis. Nat Commun. 2022 Aug 30;13(1):5105. Available from: doi: 10.1038/s41467-022-32455-1.
17. Chen, Y, Jiang Q, Peierdun M, Takiff H. E, Gao Q. The Mutational Signatures of Poor Treatment Outcomes on the Drug-Susceptible Mycobacterium Tuberculosis Genome. Elife 2023; 12: 1–13. Available from: doi.org/10.7554/eLife.84815.
18. Turon G, Hlozek J, Woodland JG, Kumar A, Chibale K, Duran-Frigola M. First fully-automated AI/ML virtual screening cascade implemented at a drug discovery centre in Africa. Nat Commun. 2023 Sep 15;14(1):5736. Available from: doi: 10.1038/s41467-023-41512-2.
19. Upadhayay A, Ling J, Pal D, Xie Y, Ping FF, Kumar A. Resistance-Proof Antimicrobial Drug Discovery to Combat Global Antimicrobial Resistance Threat. Drug Resist. Updat. 2023;66(September2022):100890. Available from: doi.org/10.1016/j.drup.2022.100890.
20. Cook GM, Hards K, Dunn E, Heikal A, Nakatani Y, Greening C, Crick DC, Fontes FL, Pethe K, Hasenoehrl E, Berney M. Oxidative Phosphorylation as a Target Space for Tuberculosis: Success, Caution, and Future Directions. Tuberc. Tuber. Bacillus Second Ed. 2017;5(3):295–316. Available from: https://doi.org/10.1128/9781555819569.ch14.
21. Anand P, Akhter Y. A Review on Enzyme Complexes of Electron Transport Chain from Mycobacterium Tuberculosis as Promising Drug Targets. Int. J. Biol. Macromol. 2022; 212 (May):474–494. Available from: doi.org/10.1016/j.ijbiomac.2022.05.124.
22. Walker JE. The NADH:ubiquinone oxidoreductase (complex I) of respiratory chains. Q Rev Biophys. 1992 Aug;25(3):253-324. Available from: doi: 10.1017/s003358350000425x.
23. Birhanu AG, Gómez-Muñoz M, Kalayou S, Riaz T, Lutter T, Yimer SA, Abebe M, Tønjum T. Proteome Profiling of Mycobacterium Tuberculosis Cells Exposed to Nitrosative Stress. ACS Omega. 2022;7(4):3470–3482. Available from: doi.org/10.1021/acsomega.1c05923.
24. Płocińska R, Wasik K, Płociński P, Lechowicz E, Antczak M, Błaszczyk E, Dziadek B, Słomka M, Rumijowska-Galewicz A, Dziadek J. The Orphan Response Regulator Rv3143 Modulates the Activity of the NADH Dehydrogenase Complex (Nuo) in Mycobacterium Tuberculosis via Protein–Protein Interactions. Front. Cell. Infect. Microbiol. 2022;12 (June):1–18. Available from: doi.org/10.3389/fcimb.2022.909507.
25. Kelam LM, Wani MA, Dhaked DK. An update on ATP synthase inhibitors: A unique target for drug development in M. tuberculosis. Prog Biophys Mol Biol. 2023 Jul-Aug;180-181:87-104. Available from: doi: 10.1016/j.pbiomolbio.2023.04.009.
26. Goedken ER, Argiriadi MA, Dietrich JD, Petros AM, Krishnan N, Panchal SC, Qiu W, Wu H, Zhu H, Adams AM, Bodelle PM, Goguen L, Richardson PL, Slivka PF, Srikumaran M, Upadhyay AK, Wu B, Judge RA, Vasudevan A, Gopalakrishnan SM, Cox PB, Stoll VS, Sun C. Identification and Structure-Based Drug Design of Cell-Active Inhibitors of Interleukin 17A at a Novel C-Terminal Site. Sci. Rep. 2022;12(1):1–12. Available from: doi.org/10.1038/s41598-022-18760-1.
27. Yu W, Mackerell AD. Computer-Aided Drug Design Methods. Methods Mol. Biol. 2017; 1520:85–106. Available from: doi.org/10.1007/978-1-4939-6634-9_5.
28. Almihyawi RA. H, Naman ZT, Al-Hasani HMH, Muhseen ZT, Zhang S, Chen G. Integrated Computer-Aided Drug Design and Biophysical Simulation Approaches to Determine Natural Anti-Bacterial Compounds for Acinetobacter Baumannii. Sci. Rep. 2022;12 (1):1–14. Available from: doi.org/10.1038/s41598-022-10364-z.
29. Stefanović C, Hager-Mair FF, Breslmayr E, López-Guzmán A, Lim C, Blaukopf M, Kosma P, Oostenbrink C, Ludwig R, Schäffer C. Molecular modelling and site-directed mutagenesis provide insight into saccharide pyruvylation by the Paenibacillus alvei CsaB enzyme. Sci Rep. 2023 Aug 17;13(1):13394. Available from: doi: 10.1038/s41598-023-40072-1.
30. Harrison C. Homology Model Allows Effective Virtual Screening. Nat. Rev. Drug Discov. 2011;10 (11): 816–816. Available from: doi.org/10.1038/nrd3597.
31. Gniado N, Krawczyk-Balska A, Mehta P, Miszta P, Filipek S. Protein Homology Modeling for Effective Drug Design. Methods Mol Biol. 2023;2627:329-337. Available from: doi: 10.1007/978-1-0716-2974-1_18.
32. Gasteiger E, Gattiker A, Hoogland C, Ivanyi I, Appel RD, Bairoch A. ExPASy: The Proteomics Server for in-Depth Protein Knowledge and Analysis. Nucleic Acids Res. 2003; 31 (13): 3784–3788. Available from: doi.org/10.1093/nar/gkg563..
33. UniProt Consortium. UniProt: the Universal Protein Knowledgebase